



HAL
open science

Assessment of fatigue crack closure phenomenon in damage tolerant aluminium alloy by in situ high-resolution synchrotron x-ray microtomography

H. Toda, Ian Sinclair, Jean-Yves Buffiere, Eric Maire, T. Connolley, M. Joyce, K.H. Khor, P. Gregson

► To cite this version:

H. Toda, Ian Sinclair, Jean-Yves Buffiere, Eric Maire, T. Connolley, et al.. Assessment of fatigue crack closure phenomenon in damage tolerant aluminium alloy by in situ high-resolution synchrotron x-ray microtomography. Philosophical Magazine, 2003, 83 (21), pp.2429-2448. 10.1080/1478643031000115754 . hal-00475153

HAL Id: hal-00475153

<https://hal.science/hal-00475153>

Submitted on 17 May 2023

HAL is a multi-disciplinary open access archive for the deposit and dissemination of scientific research documents, whether they are published or not. The documents may come from teaching and research institutions in France or abroad, or from public or private research centers.

L'archive ouverte pluridisciplinaire **HAL**, est destinée au dépôt et à la diffusion de documents scientifiques de niveau recherche, publiés ou non, émanant des établissements d'enseignement et de recherche français ou étrangers, des laboratoires publics ou privés.



Distributed under a Creative Commons Attribution 4.0 International License

Assessment of fatigue crack closure phenomenon in damage tolerant aluminium alloy by in-situ high-resolution synchrotron X-ray microtomography

H. Toda ^{a,c}, I. Sinclair ^a, J.-Y. Buffière ^b, E. Maire ^b, T. Connolley ^{a,d}, M. Joyce ^a,
K. H. Khor ^a, P. Gregson ^a

^aMaterials Research Group, School of Engineering Sciences, University of Southampton, Highfield Southampton SO17 1BJ, UK (e-mail: I.Sinclair@soton.ac.uk, tel: +44-2380-595095, fax: +44-2380-593016 (I.Sinclair))

^bGEMPPM UMR CNRS 5510, INSA, Lyon, 20 Av. A Einstein 69621 Villeurbanne Cedex, France

^cOn leave from Department of Production Systems Engineering, Toyohashi University of Technology, Toyohashi AICHI 441-8580, Japan (e-mail: toda@tutpse.tut.ac.jp, tel: +81-532-44-6697, fax: +81-532-44-6690)

^dPresent address: Industrial Research Ltd., Gracefield Road PO Box 31-310 Lower Hutt 6009, New Zealand

Abstract

Synchrotron X-ray microtomography has been utilized for the in-situ observation of steady state plane strain fatigue crack growth. A high resolution experimental configuration and phase contrast imaging technique have enabled the reconstruction of crack images with an isotropic voxel with a 0.7 μm edge. The details of a crack are readily observed, along with evidence of the incidence and mechanical influence of closure. After preliminary investigations of the achievable accuracy and reproducibility, a variety of measurement methods are used to quantify crack opening displacement (COD) and closure from the tomography data. Utilization of the physical displacements of microstructural features is proposed to obtain detailed COD data, and its feasibility is confirmed. Loss of fracture surface contact occurs gradually up to the maximum load. This is significantly different from tendencies reported where a single definable opening level is essentially assumed to exist. The closure behaviour is found to be attributable mainly to remarkable generation of mode III displacement which may be caused by local crack topology. Many small points of closure still remain near the crack-tip, suggesting that the near-tip contact induces crack growth resistance. The effects of overloading are also discussed.

Keywords: Fatigue; Crack closure; X-ray tomography; Synchrotron; Crack opening displacement; Microstructure; 2024 alloy

1. Introduction

Fatigue crack closure behaviour has been recognized as a predominant factor determining fatigue crack growth rates via shielding the transmission of external loading to a crack-tip (Elber 1971, Endo *et al.* 1972, Suresh 1981, Suresh 1996). The various mechanisms of closure, such as plasticity induced crack closure (Elber 1971), roughness induced crack closure, etc., have been discussed separately, based on very simple interpretations of the phenomena. Recently, however, one of the authors (I.S.) has examined closure processes in deflected cracks based on two-dimensional numerical simulations encompassing both plasticity and roughness contributions to closure (Parry *et al.* 2000). It has been clarified that local crack topology has significant effects on roughness induced crack closure levels due to the existence of residual plastic strains near asperity tips. To understand the absolute contribution of crack closure mechanisms to fatigue properties, the extension of two dimensional model understanding, which has been considered within the current literature, to three dimensions is clearly valuable. Nevertheless, within the available experimental literature, the three-dimensional viewpoint has been largely neglected. Since such three-dimensional crack closure behaviour is hardly approached, neither by *post failure* analyses such as fracture surface observation, nor by conventional in-situ surface observation, it would appear that in-situ X-ray tomography provides a unique possibility to assess crack closure processes.

X-ray computed tomography has been utilized as an advanced technique of diagnostic radiology in the medical field. In this case, typical spatial resolution would be up to a few hundred micrometers. Recently, third-generation synchrotron radiation facilities have been identified as an ideal source for X-ray tomography providing a high energy X-ray beam with excellent lateral coherence and monochromaticity. Microtomography performed utilizing synchrotron radiation facilities has enabled a reconstruction of volumes with a typical spatial resolution of 6.5 ~ 14 μm (Baruchel *et al.* 2000). Synchrotron X-ray microtomography has been successfully applied to studies in material science and mechanical engineering, such as characterizing the semi-solid microstructure of cast aluminium alloys (Baruchel *et al.* 2000), quantifying damage evolution in SiC reinforced metal matrix composites (Hirano *et al.* 1995, Cloetens 1997, Baruchel *et al.* 2000), observing grain boundaries in polycrystalline aluminium (Baruchel *et al.* 2000), and investigating fatigue crack closure behaviour of high

strength aluminium alloys (Güvenilir 1998, Güvenilir 1999).

In terms of the application of synchrotron X-ray microtomography to mechanical damage and crack problems, Buffière et al. (Cloetens 1997) and Stock and co-workers (Güvenilir 1998) have claimed that it can be possible to detect high contrast features occupying areas as small as one-tenth of a voxel size. This corresponds to crack opening slightly greater than $0.5\ \mu\text{m}$ for typical isotropic voxels ($6.0 - 6.6\ \mu\text{m}$) (Cloetens 1997, Güvenilir 1998), which is reasonable to detect the incidence of microscopic damage events to some extent. On the other hand, in terms of morphology and quantification, where crack topology, crack opening displacement (COD) and other features are important issues, voxel size is directly reflected in their accuracy, requiring sub-voxel interpolation (Güvenilir 1998, Güvenilir 1999) to be used especially when cracks in high strength and poor toughness materials are analysed.

For example, in the previously mentioned studies (Güvenilir 1998, Güvenilir 1999), Stock and co-workers have succeeded in the reconstruction of undisturbed three-dimensional crack surface images as a function of load by in-situ X-ray microtomography for the first time, by which the physical roles of asperity contact were interpreted via 3D images. However, an average crack opening at the maximum load was about $4\ \mu\text{m}$ in their study, which corresponds to about 60 % of voxel size ($6.4\ \mu\text{m}$), i.e. sub-voxel interpolation required to obtain any information from the results. For example, the fractions of crack opening was estimated for voxels which could be considered partially occupied by cracks, and then summed in the opening direction to calculate COD of a single crack. Differentiation of the crack from the matrix may be identified as somewhat arbitrary due to the lack of physical meaning of a threshold linear attenuation coefficient used. Handling of other factors, such as noise, interface fringes due to phase contrast and other artifacts, etc, which would be directly reflected in COD in their procedure, was not specifically described in their papers. Given their optical setup, particularly sample/detector distance (50mm), is analogous to that of the present study, the effects of phase contrast may well be significant.

In synchrotron X-ray microtomography, where a two-dimensional detector array is used to reconstruct volumetric images, the major factors affecting the spatial resolution in the reconstructed image are the pixel size and the number of pixels of a CCD detector, optical magnification, the performance of the optical setup and the use of phase contrast imaging. Owing to recent developments in optical systems (Labiche 1996, Koch 2000), an order of magnitude improvement in resolution has been enabled over the aforementioned studies. This remarkable improvement has enhanced the quality of reconstructed images and the accuracy of subsequent quantitative analyses, bringing a wider range of potential application of the synchrotron X-ray microtomography to light.

It is the objective of the present study to investigate the fatigue crack closure behaviour utilizing synchrotron X-

ray microtomography with enhanced resolution levels. A commercial high strength aluminium alloy developed for damage tolerant airframe applications (AA024-T351) was used in the experiments. High-resolution synchrotron X-ray microtomography with submicrometer voxel sizes has recently been applied to the observation of fatigue cracks (Ludwig 2002). The present paper provides the first quantitative evaluation of a cracked medium from such high resolution imaging. In order to demonstrate the effectiveness of the high resolution measurement, a variety of measurement methods are demonstrated to extract quantitative information from the tomography data. Especially, the high resolution imaging readily enables the visualisation of minute microstructural features providing a unique possibility to assess the mixed-mode (I, II and III) nature of crack opening behaviour (Anderson 1995). This is clearly advantageous compared to limited analysis procedures available in the current literature (Minakawa 1981, Allison 1988) where relatively inaccurate mode I analyses have been performed as mentioned above. Advantages and disadvantages of the respective methods are discussed with respect to accuracy and feasibility for displacement mapping, together with the results of some preliminary investigations.

2. Experimental procedure

2.1 Sample preparation

For tomographic reconstruction, an entire sample has to fit laterally into field of view. Due to the camera pixel size of a CCD camera used (i.e. 14 μm) and the optical magnification needed to obtain an isotropic voxel with a sub-micron edge, the test sample was required to be less than 1.43 mm in cross-section at maximum in this study. In order to obtain meaningful information from such a small sample, a standard sized fatigue specimen was prepared using ordinary laboratory apparatus, with a small parallelepiped specimen then being carefully extracted at the crack-tip of the original fatigue specimen to produce a steady state fatigue crack for tomographic imaging.

The overall specimen preparation was carried out as follows: 40 mm thick rolled plates of damage tolerant Al-Cu-Mg alloy, designated as 2024-T351 were utilised. Conventional single-edge notched (SEN) specimens of $5 \times 20 \times 130$ mm were produced from the centre of the plates in the L-T orientation. A slit with an approximate tip radius of 0.15 mm was machined using an EDM wire eroder giving a ratio of nominal width, W , to initial crack length, a_0 , at the onset of testing of 0.25.

Three point bend fatigue tests were carried out at room temperature in air, using an INSTRON 8872 servo-hydraulic fatigue testing machine, applying sinusoidal loading, with a load ratio, $R = P_{min} / P_{max}$, of 0.1, at a

frequency of 50 Hz. Four-point probe direct current potential drop was used for crack monitoring in all cases. Specimens were pre-cracked at a constant ΔK of 10 MPa $\sqrt{\text{m}}$ for a length of 1mm. Subsequently load shedding according to ASTM E647-95A was employed to reduce the ΔK level to 6 MPa $\sqrt{\text{m}}$ (ASTM 1995). Fatigue cracks were then allowed to grow under constant ΔK conditions at this level until a further 0.5 mm of growth had been made. The specimens prepared in this way are specified as ‘N’ (**N**ormal sample). A second set of samples was prepared in the same manner, however on completion of the process detailed above, a single 66% overload (i.e. to a maximum K of 10.0 MPa $\sqrt{\text{m}}$) was applied. The loading then reverted to the constant $\Delta K = 6$ MPa $\sqrt{\text{m}}$ baseline. Fatigue cracks were found to arrest almost immediately post overload (after ~ 50 μm of crack growth) and the tests were terminated. This second set of specimens was specified as ‘O’ (**O**verloaded sample). In the present study, only the second dataset will be discussed since space is limited. The detailed assessment of the effects of overloading will appear elsewhere in an accompanying paper (Toda 2003).

Small crack-tip samples were then prepared from the crack-tip at the original sample centre using a slow speed diamond saw. Crack-tip samples had a typical squared cross section of 0.8×0.9 mm², and a length of about 25 mm such that the longitudinal axis of the tomography specimen was parallel to that of the original specimen loading and an original crack-tip was located in it. a/W (a : crack length, W : width) of the tomography specimen was 0.68 on average. Note that since $2.5(K_{max}/\sigma_y)^2 \sim 500$ μm (σ_y : yield stress) for the maximum load, the plane strain condition should still predominate extensively for subsequent tomography observations. Finally, two epoxy end tabs were bonded at each end to make the sticklike specimens double shouldered for loading in the synchrotron experiments.

2.2 Tomographic imaging

High resolution X-ray tomography was performed at the X-ray imaging and high-resolution diffraction beamline, ID-19, of the European Synchrotron Radiation Facility (ESRF) in Grenoble, France. A material test rig was specially designed by one of the authors (J.Y.B.) for X-ray microtomography using a PMMA tube as a load frame, which gives negligible X-ray absorption (Buffière 1999). This rig was set approximately 140 m from the X-ray source ($\phi \sim 100$ μm). A monochromatic X-ray beam having a photon energy of 20 keV from a vertical multilayer monochromator was used for the experiments, giving an transmitted/incident intensity ratio of at least 10 %. A cooled 2048×2048 element CCD detector was positioned 50 mm behind the sample, thereby setting the

imaging system sensitive to phase modulation in addition to classical absorption contrast (Raven 1996). In total 1,500 radiographs, scanning 180 degrees, were taken along the loading axis at 0.12 degree increments for each load level. The whole cross section of the specimens, and a height of 210 - 280 μm was entirely captured on the CCD camera. Each view required 0.7 seconds to acquire the image: as such each full tomographic scan required at least 17.5 minutes. A first scan of the tomography was performed without loading. Scans were performed at successive 20 % increments of K_{max} . Although the load frame and the specimen were stabilized before every measurement, stress relaxation of the order of ~10 % of applied load was observed during some scans. Image slices were reconstructed from the series of projections based on a conventional filtered backprojection algorithm (Herman 1980). Grey value in each dataset was calibrated so that variation between the most opaque and transparent voxels could be expressed within an 8 bit grey scale range between 0 and 255. Isotropic voxel with a 0.7 μm edge was achieved in the reconstructed slices. By analogy with previous reports (Cloetens 1997, Guvenilir 1998), substantial detectability for a crack is expected to approach 0.05 μm . Details of the experimental scheme and setup are more fully described elsewhere (Cloetens 1997, Buffière 1999).

2.3 Volume rendering

As noted earlier, a key point in the present paper is the analysis of various methods by which quantitative information on crack opening may be extracted from tomographic data. To perform such quantitative analyses, the identification of object volumes (particles or cracks) via some form of grey scale imaging is clearly significant. As with all image analysis, careful assessment of thresholding criteria and accurate reflection of the feature of interest is required.

In order to evaluate CODs in the cracked samples, the tomographic dataset was thresholded and labelled utilizing a grey value for each 3D feature of interest (i.e. the crack at a given load level or a microstructural feature in the bulk metal). Firstly the feature of interest was chosen on some two-dimensional reconstructed slice, and a three-dimensional 'seed' growth technique was applied to identify the volume of the feature. All voxels that are three-dimensionally connected to the manually set seed point and have a voxel grey value within a set tolerance range are thresholded and labelled as one feature. Volume, surface area and centre of gravity measurement of each feature were automatically measured using dedicated software developed at Luc Salvo lab. GPM2 INP Grenoble. To estimate fracture surface areas at sub-voxel accuracy, pentagonal faceted iso-intensity surfaces were computed from the volumetric data set by a conventional Marching Cubes algorithm (Lorenson 1987).

As an initial analysis, the volume of whole or partly extracted cracks was divided by their projected area to obtain an average crack opening displacement. The ‘extracted’ crack here means the open volume between the two crack faces, as thresholded by the above method. COD measurements were sought at scales of the order of one voxel size, using two-dimensional representations of spatial distribution of opacity. Such measurements were produced by a direct ray casting technique (Roth 1982) over the whole crack. A notional ray of light is cast from a viewpoint perpendicular to the crack plane through each voxel of the segmented crack, projecting an overall opacity onto a plane perpendicular to the loading axis. The final grey scale distribution for the resultant projected 2D image of the crack corresponds to accumulating opacity values along the rays. All the voxels which belonged to the crack are set fully opaque before the projection using a simple boxcar transfer function (Jani 1998) so that the total opacity along a given ray through the crack gives quantitative information on the local thickness of the thresholded volume. This representation enables two-dimensional mapping of COD values over the whole crack surface. In terms of the accuracy of these measurements, the so-called partial volume effect (Labbe 1996) is crucial, which brings a transition area with a grey value ramp over several voxels in width at an interface between radiographically dissimilar phases. Provided that the tolerance value applied is appropriate, the partial volume effect can cause an error of half the voxel size at maximum (i.e. less than 0.35 μm in this study) in the local COD measurement when the feature of interest is as small as one voxel square. Errors at respective voxels are equalized in the calculation of the average COD value, whereas the local COD value obtained by the ray casting technique can give relatively inaccurate data, depending on an absolute COD value. Half the voxel size corresponds to approximately 5 and 17 % of average COD values calculated over a distance of 7 μm from the crack-mouth and the crack-tip, respectively. To reduce such error, COD values were averaged over four voxels when constructing a given COD profile. Note that the existence of such errors has no relation to reproducibility in the COD measurements. As far as a specific set of setting values (such as thresholding tolerance) is used, a unique COD value is obtained from a sequence of operations.

To overcome the above shortcomings, a further COD quantification method may be identified, where secondary phase bodies within the material microstructure may be used as displacement gauges by which compliance of the underlying material is measured at a microstructural scale. Firstly, a pair of spherical microstructural features, such as intermetallic compounds or micro-pores within the material, are sampled as gauge marks so that these are located on opposite crack faces, lying approximately parallel to the loading axis. Variations during loading in the centroid spacings of such particle pairs may then be separated into three directions by orthogonal decomposition. Although this procedure does not give absolute values of COD, there are several valuable features: such as (a)

mode I, II and III displacement components can be assessed, which can not be drawn from the previously referenced methods, (b) partial volume effects can be minimized by utilizing symmetric particles or micro-pores, and (c) more robust automatic displacement mapping can potentially be constructed as a function of local crack topology (especially in the case of aluminium alloys in which many kinds of coarse intermetallic compound particles are densely dispersed, enabling a detailed mapping procedure).

3. Results and discussion

3.1 Object thresholding

[Insert figure 1 about here]

Figure 1 shows a 2D slice of a reconstructed volume which contains a crack, micro-pores (shown in black: less than 1 μm) and intermetallic compound particles (shown in white: typically Fe-rich $\beta\text{-Al}_7\text{Cu}_2\text{Fe}$, but may contain some S, η and some other Si-rich phases.). Owing to the high resolution optical setup, not only the crack but also microstructural features of the aluminium can be clearly visualised. The image of this virtual slice is as distinct, offering similar detail as a high magnification optical microscope image (i.e. resolutions are of a similar order and similar contrasting of the main features may be obtained). In all cases, cracks were seen to be predominantly open, even at the minimum applied load. Crack bifurcation and serrated crack paths are readily observable at points A and B, respectively in figure 1. Furthermore, crack closure contact can be clearly observed at C. It may be noted that the crack does not appear completely black by comparison to the micro-pores. Figure 2 illustrates grey value profiles of the crack along transverse lines (a) near the crack-mouth and (b) crack-tip. Distinct light and dark fringes at each crack edge can particularly be seen in figure 2 (a) and (b) due to phase contrast effects between the air and aluminium (Cloetens 1997). Average grey values at the minimum load of the aluminium and crack volumes were 190.4 and 95.1, respectively. The fringes generated by phase contrast at the crack edges were seen to exert a strong influence on the grey value of the crack region. The contrast value corresponding genuinely to X-ray absorption in air would in fact be close to that of the crack centre near the crack-mouth (i.e. 130~150). The particular darkness of the micro-pores and the near tip crack volume (in figure2 (a)) is particularly attributable to the dark fringes (associated with interface phase contrast) overlapping in such small objects.

[Insert figure 2 about here]

[Insert figure 3 about here]

Given the above contrast effects, a key issue in thresholding the crack in a reconstructed volume is the optimum threshold selection. Considering the partial volume effect, it is interesting to adopt a mean value between the grey values of neighbouring two phases as a threshold value to determine the location of an associated interface. Such mean contrast values were identified as 144.9 and 143.5 for near the crack-tip and the whole crack respectively. However, voxel contrast values slightly exceed these mean values near the crack centre, which means that the thresholded volume of a crack (and hence measured COD) should be significantly underestimated if such a mean value is applied for thresholding. This is illustrated in figure 3 where approximately linear variations of the volume and surface area of a segmented crack are seen with thresholding tolerance values increasing between 120 ~ 160. The crack surface area corresponds to the area of fracture surface which is apparently open at a given load level. The increment in the crack volume during whole the linear portion is about 184 %, while that of the crack surface area is ~ 35 %. It can be inferred that the high grey value region at the crack centre becomes filled (i.e. becomes part of the thresholded volume) with increasing threshold tolerance. Since the upper bound grey value of the linear portion exceeded that of the internal high grey value region almost all over the crack, adopting the onset of non-linearity of the upper part as a tolerance value in figure 3 seems to give reasonable thresholding. In fact, changing the tolerance value from 143.5 (i.e. the above-mentioned mean grey value at an interface) to 160 (i.e. uppermost value in figure3) resulted in expansion of the crack volume by ~ 0.057 μm , which brought about the increase in crack surface area by 0.7 (at P_{max}) ~ 7.7 (at P_{min}) %. This means that computation errors in CODs caused by adopting the larger tolerance value are less than 3 % for a crack-tip, and less than 1 % on average, which are significantly smaller than the variations observed in figure 3. Thus, a thresholding tolerance value of 160 was adopted for the dataset illustrated in figure 3, with a similar determination process being applied separately for each dataset. Average COD values measured by this volume-based procedure showed an excellent agreement with those from the ray casting technique. For example, the former for the dataset illustrated in figure 3 was 5.79 μm at the maximum load, while the latter for the same dataset was 5.71 μm .

As shown above in figure 3, measured object volume increases with the increase in tolerance value, however the centroid location is essentially unchanged. In fact, changing the threshold tolerance value by 20 results in an absolute shift in the measured centre of gravity of the particle of only 0.043 μm on average and 0.139 μm at most, indicating that this procedure brings about one order of magnitude improvement in displacement measurements over the crack volume-based measurements. It is concluded that the utilization of centroid spacings of such spherical microstructural features as a displacement gauge may lead to reliable and robust COD measurements, relatively independent of the thresholding conditions: such stability may be seen to enable automatic accurate

COD mapping when a suitable population of particles is identified.

3.2 General features of 3D rendered image

[Insert figure 4 about here]

Figure 4 (a) shows part of a rendered volume ($200 \times 300 \times 200$ voxels) encompassing a crack-tip: within this volume the crack has been visualized by removing underlying aluminium from two-thirds of its volume. Completely black spherical micro-pores, coarse and irregular intermetallic compound particles (which appear light grey) and a neutral-coloured crack (i.e. the open portion of the crack) can be observed in the diagram. These phases were rendered using front and side diffuse light sources to highlight their three-dimensional character (Sassen 1991). The geometry of the crack's leading edge, and the surface topology of the crack are complex and three-dimensional. As can be seen in figure 4 (b), which shows a view of the crack diagonally from the rear, bifurcated crack planes C1 and C2 are connected by a segment of the crack plane T which twisted about the crack growth direction. Crack plane C2 is located approximately $40 \mu\text{m}$ beneath C1, with the two areas overlapping each other. There seems to be some crystallographic effects on the formation of the bifurcation. Although it has not been investigated in the present study, one of the advantages of the X-ray microtomography is three-dimensional grain boundary mapping utilizing Gallium wetting techniques (Ludwig 2002). Such an investigation can give a more definitive metallurgical insight in the tomographic image. In the first instance, it may still be seen from the present results that even though bifurcation may look simple on two-dimensional slices, three-dimensional observation reveals that multiple crack planes were involved in crack growth, probably intricately interacting with underlying grain structure.

The complex shape and scale of the intermetallic particles is clear from the 3D reconstruction, highlighting the limited impression obtained from 2D sections. The intermetallic particles seen in the immediate vicinity of the crack in this work remained intact, indicating that the effects of the particles on crack propagation was not significant for the test conditions.

The micro-pores can be divided into two families. One is associated with the brittle intermetallic particles which break during the various shaping processes which transform the ingot into plate. The other one is apparently not associated with any intermetallic particles. It may be hydrogen precipitation, but it could be also associated to small particles not visible at the $0.7 \mu\text{m}$ resolution. Although particle volume fraction and porosity (observed in figure 4 (a)) appear relatively high for a wrought aluminium alloy, this is also simply due to the

difference between the two-dimensional cross-sections and real three-dimensional materials. In fact, Martin et al. have shown that there was an excellent agreement in measured porosity values between the high resolution X-ray microtomography and Archimedean densimetry in a 5083 alloy (Martin 2000).

[Insert figure 5 about here]

Figure 5 shows a front and side illuminated rendering of the crack emphasizing the surface topology. Figure 5 (a) and (c) were captured at the minimum load, whilst figure 5 (b) was obtained at the maximum load. Several large ridges (i.e. valleys on the fracture surfaces) rise on the crack, running parallel to the crack growth direction. One relatively large ridge forks into two at the midpoint. Areas where the background colour can be seen (white) indicate the existence of crack closure or ligaments in the crack wake. Comparison of loaded and unloaded images allows the two conditions to be unambiguously identified. Areas of contact are particularly seen along the ridges and valleys behind the crack-tip, whilst small points of contact (typically $\sim 7 \mu\text{m}$) are scattered near the crack-tip as shown in figure 5 (c); relatively large regions of fracture surface contact are labelled A on figure 5(a). It is probable that such points are unbroken ligaments in the crack, however there is little evidence in the literature that ligaments of such a morphology arise in these materials. The white patches at A mostly disappear or contract to very small dots at the maximum load. On the other hand, although region A had almost lost contact, many small points of closure still remained near the crack-tip. Since such a near tip contact may directly affect local effective stress intensity range at a crack-tip, the near-tip contact seems to cause apparent benefits to fatigue crack growth resistance. Another feature to note is localized crack opening projecting sharply ahead of the general crack line with loading, as indicated by B in figure 5. Figure 6 shows a ray casting representation (Roth 1982) that represents COD distribution over the whole crack, where completely black areas correspond to zero opening (i.e. contact), whilst the lighter a voxel, the larger the opening displacement. It may be seen that crack opening is characterised by several light stripes, as indicated by arrows, which correspond to the rows of widely opened crack segments, running in the crack growth direction, alternating with dark stripes (i.e. regions where COD is zero or negligibly small). This suggests that the ridges and valleys of the fracture surface running in the crack growth direction may in fact contribute to crack closure owing to mode III displacements. Such macroscopic contact in the 'far' crack wake appears quite distinct from closure near the crack-tip ($\sim 100 \mu\text{m}$) which is dispersed irregularly, corresponding to subtle undulations of the crack plane.

[Insert figure 6 about here]

3.3 COD analyses and crack closure behaviour

[Insert figure 7 about here]

Figure 7 (a) and (b) show the variations of COD and crack surface area, respectively as a function of applied load. The crack opened almost linearly with progressive loading. This tendency was also confirmed by the centroid spacing measurement of particles and the crack volume-based measurement. The initial COD increment looks slightly smaller than those of the later stage of loading; this effect may also be identified by the other methods, as shown later in figure 8 (a) and (b). Figure 7 (b) shows characteristic behaviour that the decreasing rate of fracture surface contact (i.e. the increasing rate of crack surface area) increased exponentially with loading until $K = 2.71 \text{ MPa}\sqrt{\text{m}}$ (i.e. about 58 % of K_{max}) and then showed smaller decreasing rate above it. None of the existing macroscopic closure measurement methods (Minakawa 1981, Allison 1988), which essentially assume a single definable opening level in a load cycle has clarified such a progressive contact and loss of contact.

[Insert figure 8 about here]

[Insert figure 9 about here]

Figure 8 shows the variations of local COD with loading which were measured by the centroid spacing measurement of particles. Data which were measured in the middle of the whole crack length and at about 170 ~ 250 μm from the crack-tip are shown in figure 8 (a) and (b), respectively. Of the three points shown in figure 8 (a), point C is close to a peak of crack deflection and there is a contact point just between the two micro-pores sampled for the COD measurement. The crack is propagated almost horizontally around point A. Point B is located between two contact points due to a serrated crack path. The tendency in figure 8 is overly consistent with that of average COD by the crack volume-based measurement in figure 7 (a) except that the data for points B and C are slightly different from the others, presumably due to the effects of the contact points resulting in distorted curves and smaller increments in COD than point A. Figure 9 shows the variations of mode II and III displacements. The same points as figure 8 are sampled in the measurements. The generations of the relatively large mode III displacement of about 0.6 and 1 μm were observed for points A - C and D - F, respectively, whilst the mode II displacement was less than 0.3 μm at maximum in most cases. Points B and C, which showed the different tendencies from the other points in figure 8 and also from the average COD variations shown in figure 7 (a), show different variations in mode II and III displacements, suggesting that the variations of the mode I displacement are closely associated with mode III (and sometimes mode II) fracture surface contact. In fact, the rapid decrease of fracture surface contact was observed in figure 7 (b) up to the load level below which the mode III displacements were seen to vary significantly in figure 9 (b) (i.e. $K = 2.71 \text{ MPa}\sqrt{\text{m}}$). The larger mode III

displacements may be attributable to the features of crack surfaces shown in figure 6 where the ridges and valleys run in the crack growth direction. It may be also noted that the directions of the mode II and III displacements differ from point to point, implying that the observed mode II and III displacements are particularly attributable to the local topology of crack surfaces such as crack deflection and bifurcation and not to macroscopic factors such as the effects of the very small specimen size, misalignment of the test apparatus, etc. The dispersions of the mode I displacement curves observed in figure 8 (especially in figure 8 (a)) are deemed to represent such local characteristics of individual positions.

The COD measurement based on the centroid spacing measurement of particles may inherently include elastic and plastic deformation in the crack wake lying between the particles. Especially compression at contacting points due to asperity wedging, local residual strains arising from crack propagation process such as crack deflection, and inhomogeneous strain distribution due to rough fracture surface (i.e. strain concentration) may give rise to significant local displacements along with global deformation in the crack wake. When COD itself is a key issue, these contributions should be subtracted from measured values. Although the local COD value obtained by the ray casting technique can give relatively inaccurate data depending on voxel size, comparison of results drawn by the two methods may give a rough estimate of the fraction of such contributions. Difference in COD increments (between the minimum and maximum loads) obtained by the centroid spacing measurement and the ray casting technique showed significant dispersions ranging between 0 ~ 0.97 μm in nine measurements (which were performed at three different distances from a crack-tip: 170 ~ 250, 350 ~ 460 and 600 ~ 650 μm). This means that about 20 % of the COD values obtained by the centroid spacing measurement of particles may on average be caused by the above-mentioned local deformations in the crack wake.

[Insert figure 10 about here]

[Insert figure 11 about here]

Figure 10 shows COD profiles on two different sections by the ray casting algorithm plotted back from the crack-tip. Figure 10 (a) shows typical of profiles which compare the minimum and maximum loads. Figure 10 (b) is an enlarged profile around the crack-tip where small patches of closure are dispersed. It is clear that the increment in COD is small over about 80 μm from the crack-tip, with crack opening due to loading mainly occurring behind this region. This can be confirmed more clearly in figure 11 where average values over the whole crack are plotted as a function of distance from the crack-tip. Since the length over which opening does not occur markedly (i.e. 80 μm from the tip) is comparable to the prior plastic zone size during overloading in this sample, the characteristic opening behaviour thus seems to be associated with overloading. Possible mechanisms

for this may be enhanced plasticity induced crack closure due to the overload (von Euw 1972), roughness induced crack closure, caused by shear mismatch between the mating crack faces, and the potential combination of the two processes. This will be discussed more fully later in a companion paper (Toda 2003). As stated earlier, figure 10 (b) clearly illustrates that ridges with a large COD range along with valleys with a small COD for the minimum load, while for the maximum load, COD becomes flatter.

4. Summary

High resolution synchrotron X-ray microtomography has been utilized to perform in-situ observation of fatigue crack closure behaviour in a high strength aluminium alloy. By sampling a small tensile specimen available for the in-situ testing rig from a fatigued standard specimen, high resolution observation (isotropic voxel with a 0.7 μm edge) of a crack propagating steadily under plane strain conditions has been realized. The high resolution experimental setup and the utilization of phase contrast technique have enabled the reconstruction of the distinct 2D slices and 3D rendering of a crack, pores and intermetallic particles with excellent image quality. The details of a crack, such as its surface topology, bifurcation and crack-tip geometry, have been readily observed by volume rendering as well as by evidence of the incidence and mechanical influence of closure. This provided valuable insights into the understanding of fracture phenomena. Where and how to account such three-dimensional aspects is one of the key issues. Firstly, thresholding conditions were investigated to quantify COD and closure accurately and to secure its reproducibility. One method to quantify the surface area of a contacting crack face and three methods to draw information concerning COD from the rendered 3D images were demonstrated and their effectiveness was exhibited. The latter methods used were the crack volume-based measurements suitable to cover a relatively wide area, the ray casting technique which provided a comparatively low resolution (voxel size level) with high density mapping of COD together with closure, and the local COD measurement by the centroid spacing of marker particles. It has been clarified that the global COD measurement by the crack volume method and the local COD measurement by centroid spacing could be performed with accuracies of one order of magnitude smaller than the voxel size together with sufficient reproducibility. Especially, the latter method is considered to be a robust procedure being appropriate for automatic mapping of COD with high accuracy, providing high-density mapping especially in the case of aluminium alloys which inherently contain small but closely interspersed intermetallic particles and micro-pores. Overall, high resolution in-situ synchrotron X-ray microtomography might offer the highly effective way of assessing the fatigue problems

and provides in-situ images and quantitative information which can be drawn neither by *post failure* analyses nor by other in-situ observation procedures which are surface-based or based on other low resolution NDT techniques.

It has been clarified that loss of fracture surface contact occurred rapidly along with the decreases in mode II and/or III displacements during loading to a halfway, then more gradual loss of contact was observed until the maximum load. Such progressive loss of contact was not consistent with simplified models available in the current literature, which essentially assume a single definable opening level in a load cycle. The closure behaviour was found to be attributable mainly to remarkable generation of mode III displacement, being associated with the local crack surface topology of the test sample. Many small pieces of closure still remained near a crack-tip even at the maximum load, suggesting that the near-tip contact might cause apparent benefits to crack growth resistance. The effects of overloading were also discussed utilizing characteristic crack opening profiles obtained which showed less amount of opening over the specific distance from a crack-tip than the rest of the crack.

Acknowledgement

The ID19 staff is acknowledged for assistance during the experiment. One of the authors (H.T.) would like to acknowledge support through the JSPS - Royal Society Bilateral Programme. The support of Pechiney CRV to K.H.K. and stimulating discussions with J.C Ehrström in Pechiney CRV are also gratefully acknowledged.

References

- Allison, J. E., Ku, R. C., and Pompetzki, M. A., 1988, *ASTM STP982* (Pennsylvania: American Society for Testing and Materials). p.171.
- Anderson, T.L., 1995, *Fracture Mechanics* (Boca Raton: CRC Press), p.53.
- ASTM E647, 1995, *Annual Book of ASTM Standards, Section 3*, Vol.03.01 (Pennsylvania: ASTM), p.578.
- Baruchel, J., Buffière, J-Y., Maire, E., Merle, P. and Peix, G., 2000, *X-ray Tomography in Material Science* (Paris: Hermes Science Publications).
- Buffière, J. Y., Maire, E., Cloetens, P., Lormand, G. and Fougères, R., 1999, *Acta mater*, **47**, 1613.
- Cloetens, P., Pateyron-Salome, M., Buffière, J. Y., Peix, G., Baruchel, G., J., Peyrin, F. and Schlenker, M., 1997, *J. Appl. Phys.*, **81**, 5878.
- Elber, W., 1971, *ASTM STP486* (Pennsylvania: American Society for Testing and Materials). p.230.

Endo, K., Okada, T. and Hariya, T., 1972, *Bulletin of the Japan Society of Mechanical Engineers*, **15**, 439.

Guvencilir, A. and Stock, S. R., 1998, *Fatigue & Fract. of Engng. Mater. & Struc.*, **21**, 439.

Guvencilir, A., Breunig, T.M., Kinney, J.H. and Stock, S. R., 1999, *Phil. Trans. R. Soc. Lond.*, **A 357**, 2755.

Herman, G. T., 1980, *Image Reconstruction from Projections, The Fundamentals of Computerized Tomography* (Orland: Academic Press).

Hirano, T., Usami, K., Tanaka, Y. and Masuda, C., 1995, *J. Mater. Res.*, **10**, 381.

Jani, A. B., Pelizzari, C. A., Chen, G. T. Y. and Grzeszczuk R. P., 1998, *J. Computer Assisted Tomography*, **22**, 459.

Koch, A., Cloetens, P., Ludwig, W., Labiche, J.C., and Ferrand, B., 2000, *Proceedings of the 5th International Conference on Inorganic Scintillators and Their Applications SCINT99*, edited by Lomonosov (Moscow, Moscow State University), pp.157-166.

Labbe, C., Froment, J. C., Kennedy, A., Ashburner, J., Cinotti, L., 1996, *Alzheimer Disease & Associated Disorders*, **10**, 141.

Labiche, J. -C., Segura-Puchades, J., van Brusel, D. and J.P. Moy, 1996, *ESRF Newsletter*, **25**, 41.

Lorensen, W. E. and Cline, H. E., 1987, *Computer Graphics*, **21**, 163.

Ludwig, W., Buffière, J-Y., Savelli, S., Cloetens, P., 2002, *Acta mater*, **51**, 585.

Martin, C. F., Josserond, C., Salvo, L., Blandin, J. J., Cloetens, P. and Boller, E., 2000, *Scripta Metall.*, **42**, 375.

Minakawa, K. and McEvily, 1981, A. J., *Scripta Metall.*, **15**, 633.

Parry, M.R., Syngellakis, S. and Sinclair, I., 2000, *Mater. Sci. Engng.*, **A291**, 224.

Raven, C., Snigirev, A., Snigireva, I., Spanne, P., Souvorov, A. and Kohn, V., *Appl. Phys. Lett.*, **69**, 1826.

Roth, S. D., 1982, *Computer Graphics and Image Processing*, **18**, 109.

Sassen, K., 1991, *Bulletin of the American Meteorological Society*, **72**, 1848.

Suresh, S., 1996, eds. D.R.Clarke, S.Suresh, and I.M.Ward, *Fatigue of Materials*, edited by D.R.Clarke, S.Suresh, and I.M.Ward(Cambridge: Cambridge Solid State Science Series).

Suresh, S., Zamiski, G. F., and Ritchie, R. O., 1981, *Metall. Trans.*, **12A**, 1435.

Toda, H., Sinclair, I., Buffière, J.-Y., Maire, E., Khor, K. H., Joyce, M., Connolley, T., Gregson, P., 2003, to be submitted.

von Euw, E. F. J., Hertzberg, R. W., and Roberts, R., 1972, *ASTM STP513* (Pennsilvania: American Society for Testing and Materials). p.230.

Caption list

Fig.1 A two-dimensional slice of the reconstructed volume captured at $K = 0.42 \text{ MPa}\sqrt{\text{m}}$ corresponding to the mid-section of the rendered volume shown in Fig. 5 (a).

Fig.2 Typical variations in grey value across a crack. Original image was captured at $K = 4.69 \text{ MPa}\sqrt{\text{m}}$. Crack-tip and crack mouth were stacked for comparison.

Fig.3 The results of preliminary investigations representing the effects of tolerance value used during segmenting a crack on crack volume and crack surface area.

Fig.4 3D rendered perspective views of tomographic data taken at $K = 0.42 \text{ MPa}\sqrt{\text{m}}$, representing the vicinity of a crack-tip after aluminium has been removed from two thirds of a volume of $200 \times 300 \times 200$ voxels. Crack bifurcation is observed from the alternative angle in (b), with sections C1 and C2 of the crack overlapping each other, whilst being connected by the twisted section, T.

Fig.5 Ray tracing representations of the crack which emphasize surface topology. (a) and (b) represent the whole crack and taken at $K = 0.42$ and $4.69 \text{ MPa}\sqrt{\text{m}}$, respectively. (c) is an enlarged view of (a) including the crack-tip.

Fig. 6 Ray casting representation of the whole crack which was used for the COD mapping. The image captured at $K = 0.42 \text{ MPa}\sqrt{\text{m}}$ was used for the investigation. Arrows indicate the rows of widely opened crack segments.

Fig. 7 Variations of (a) COD averaged over the whole crack, δ_{all} , and (b) crack surface area, $2A$, normalized by projected crack area, A_p , as a function of applied stress intensity.

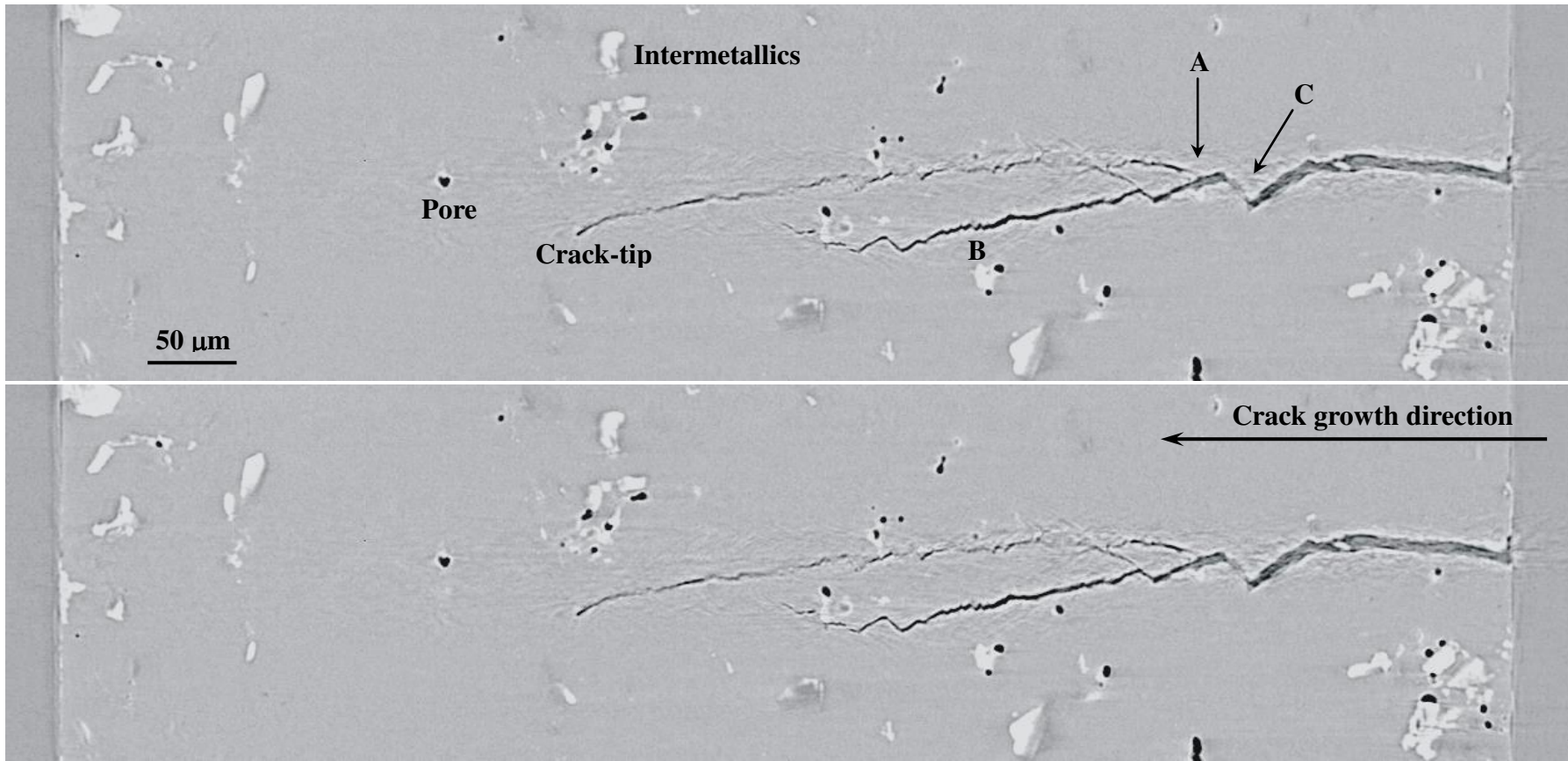
Fig.8 Variations of local opening displacement, δ_c , as a function of applied stress intensity measured utilizing centroid spacing of each pair of pores. (a) and (b) were measured about $170 \sim 250 \mu\text{m}$ and $350 \sim 460 \mu\text{m}$ from a crack-tip, respectively.

Fig.9 Variations of (a) mode II displacement, δ_{II} , and (b) mode III displacement, $|\delta_{III}|$, as a function of applied stress intensity measured utilizing centroid spacing of each pair of pores. Points A ~ F correspond to those in Fig.8 respectively.

Fig. 10 COD profiles on two different cross-sections plotted from a crack-tip backwards. The ray casting algorithm was utilized for the measurements. (a) is a typical profile almost over the whole crack, while small points of fracture surface contact were observed in the vicinity of the crack-tip in (b).

Fig. 11 COD profiles after averaging the COD data over the whole crack plotted as a function of distance from a

crack-tip.



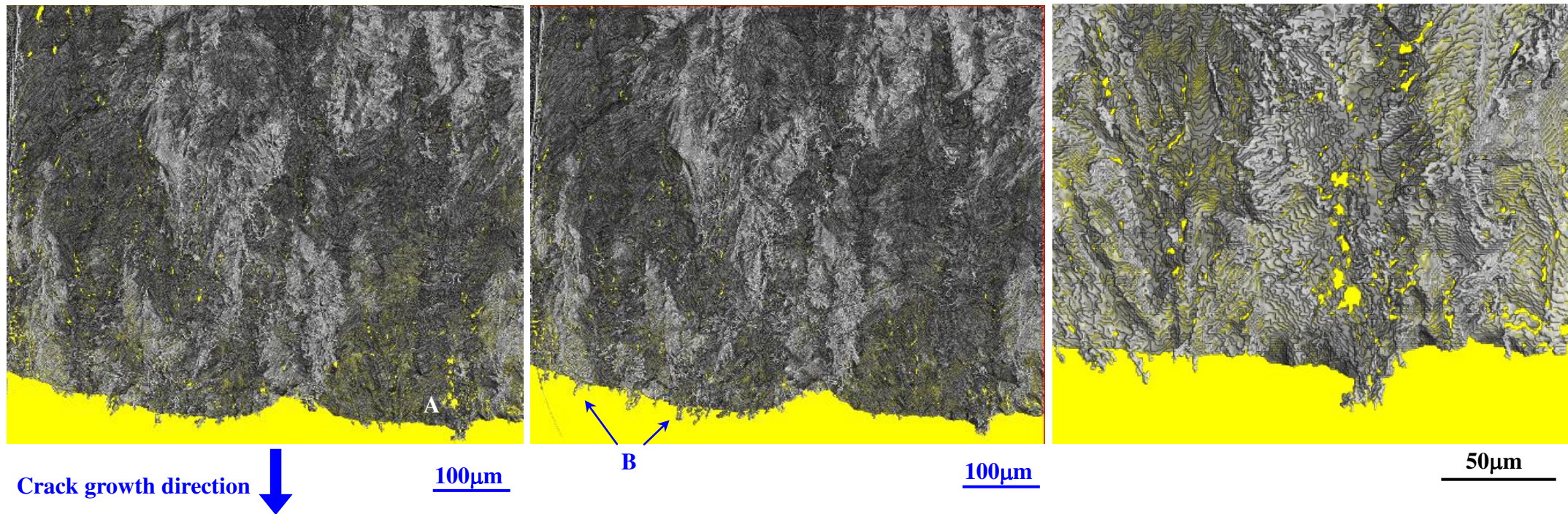


Fig.6 Ray tracing representations of the crack which emphasize surface topology. (a) and (b) represent the whole crack and taken at $K = 0.42$ and $4.69 \text{ MPa}\sqrt{\text{m}}$, respectively. (c) is an enlarged view of (a) including the crack-tip.

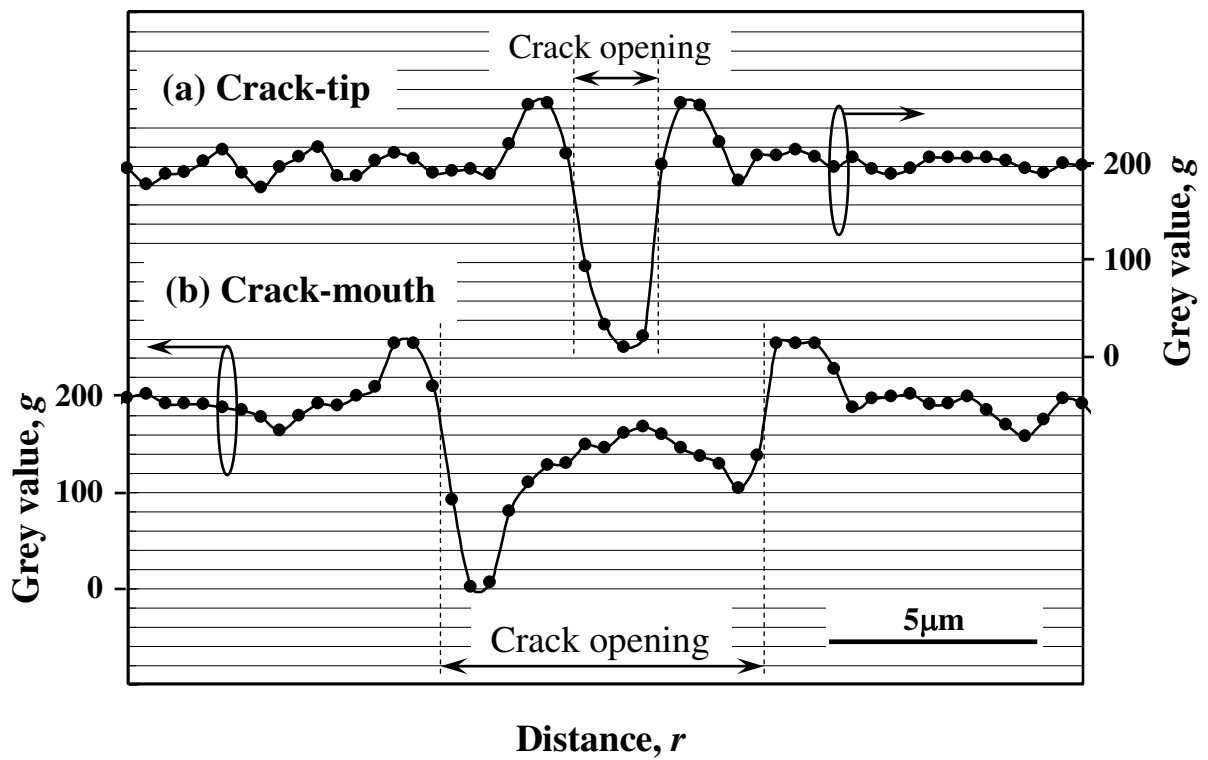


Fig.2 Typical variations in grey value across a crack. Original image was captured at $K = 4.69 \text{ MPa}\sqrt{\text{m}}$. Crack-tip and crack mouth were stacked for comparison.

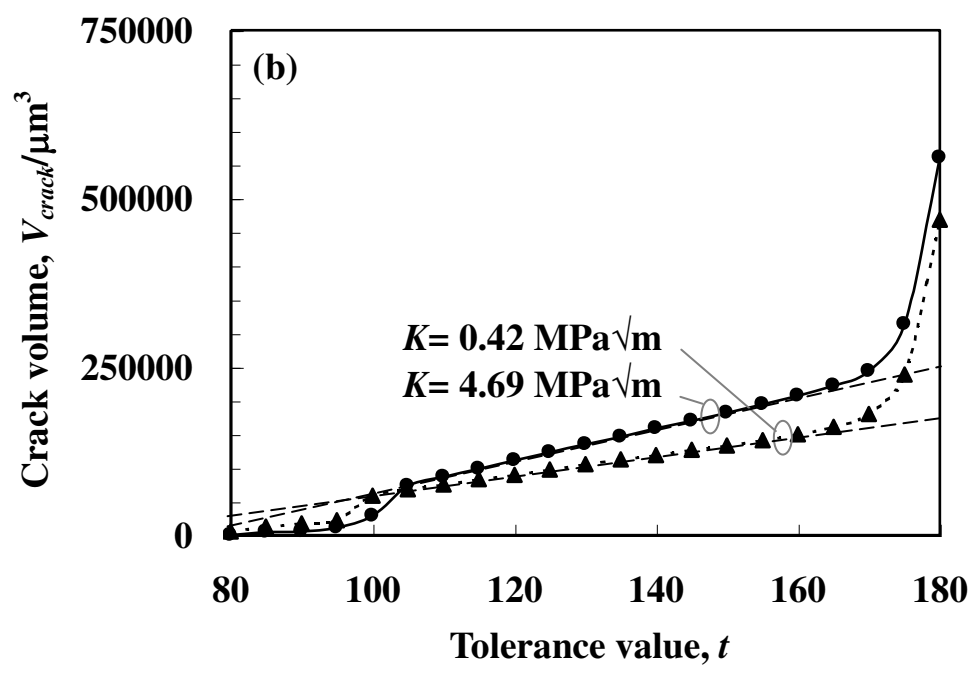
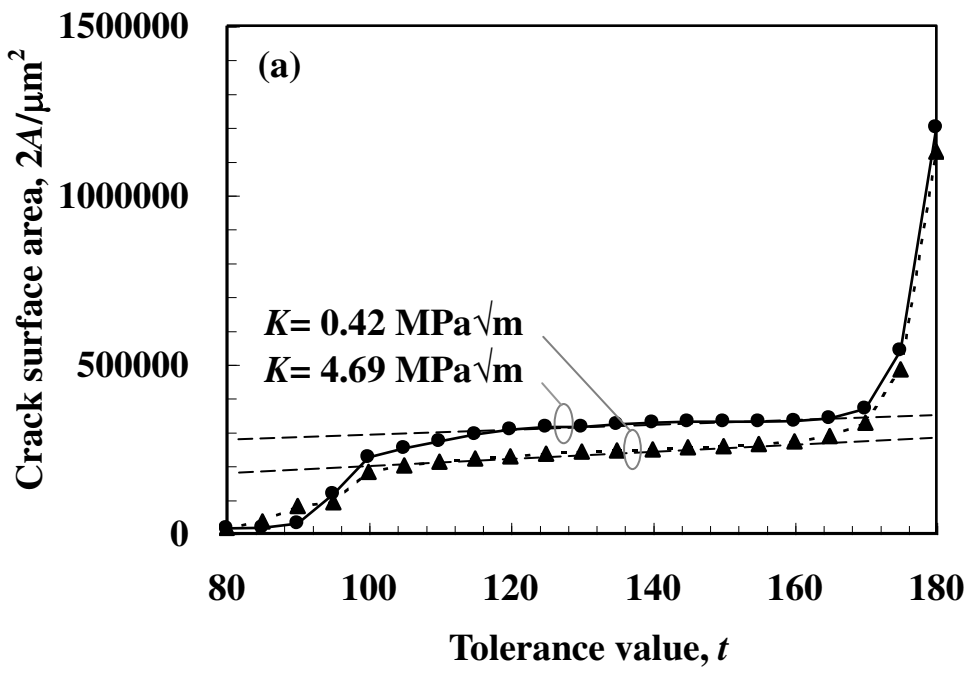


Fig.3 The results of preliminary investigations representing the effects of tolerance value used during segmenting a crack on crack volume and crack surface area.

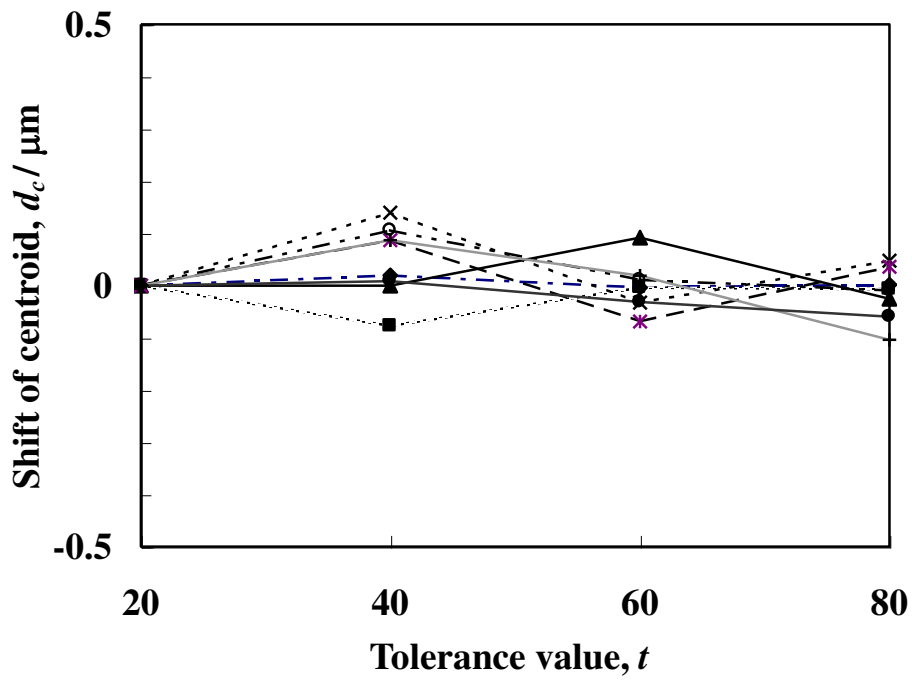
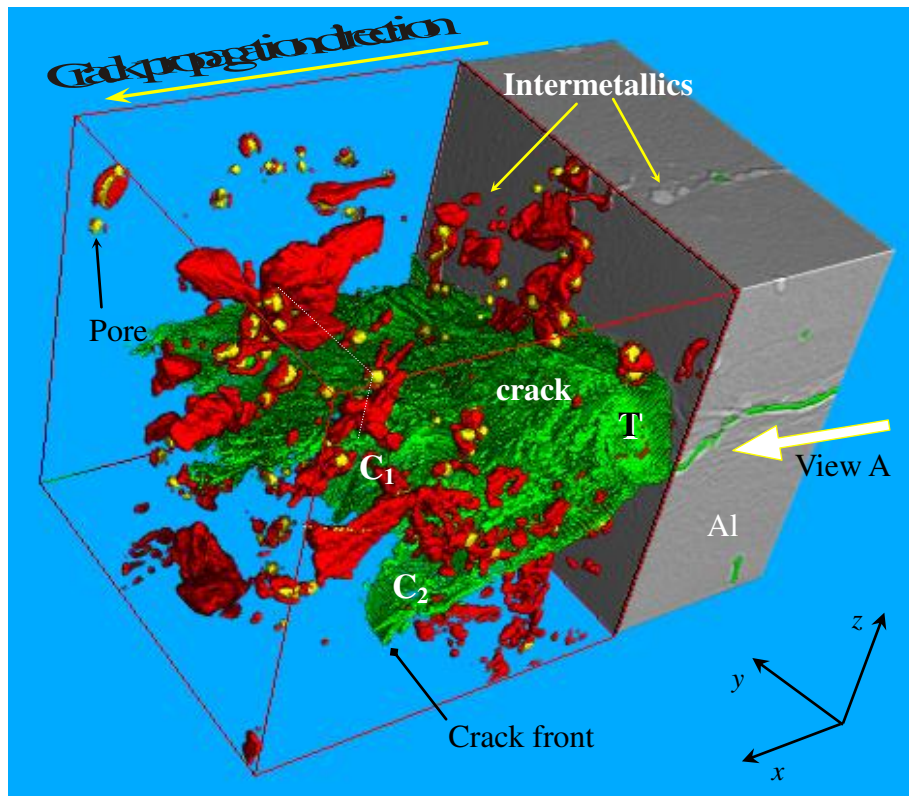
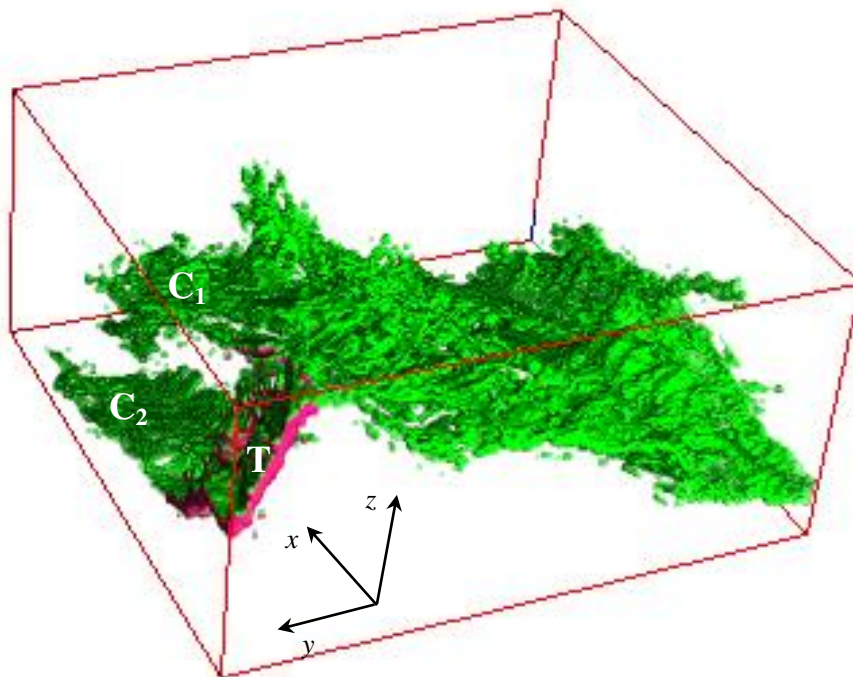


Fig.4 The effects of thresholding tolerance value in thresholding pairs of pores in terms of centroid spacings. Centroid positions determined by a threshold tolerance of 20 were used as a reference value.



(a) Extracted volume



(b) The crack in (a) viewed from direction A.

Fig.5 3D rendered perspective views of tomographic data taken at $K = 0.42 \text{ MPa}\sqrt{\text{m}}$, representing the vicinity of a crack-tip after aluminium has been removed from two thirds of a volume of $200 \times 300 \times 200$ voxels. Crack bifurcation is observed from the alternative angle in (b), with sections C1 and C2 of the crack overlapping each other, whilst being connected by the twisted section, T.

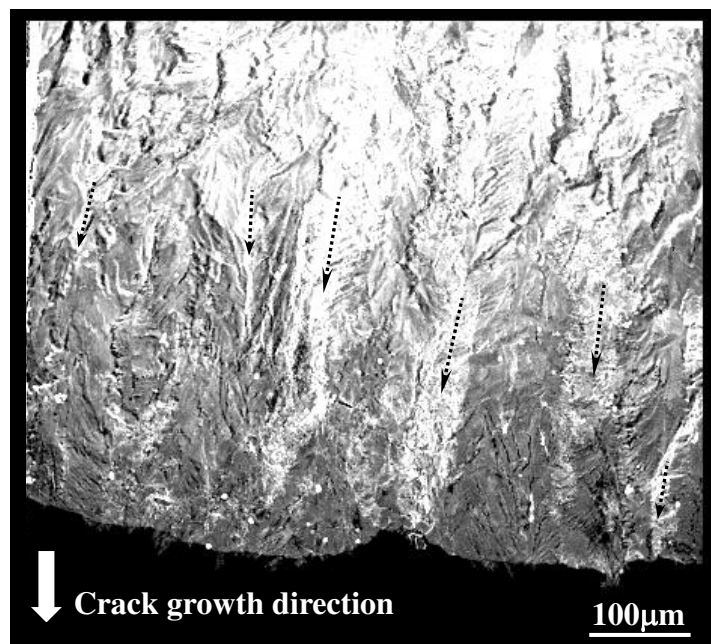


Fig. 7 Ray casting representation of the whole crack which was used for the COD mapping. The image captured at $K = 0.42 \text{ MPa}\sqrt{\text{m}}$ was used for the investigation. Arrows indicate the rows of widely opened crack segments.

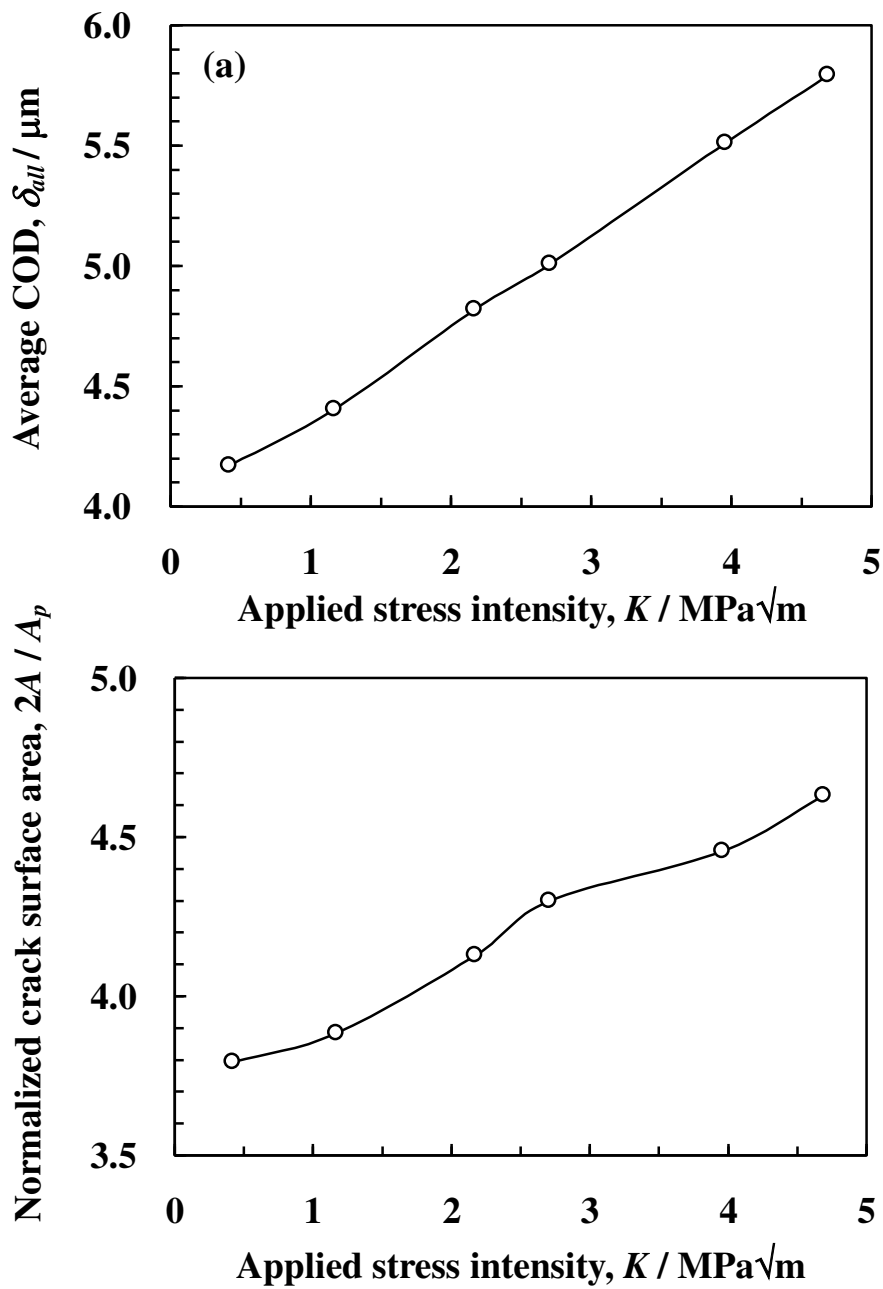


Fig. 8 Variations of (a) COD averaged over the whole crack, δ_{all} , and (b) crack surface area, $2A$, normalized by projected crack area, A_p , as a function of applied stress intensity.

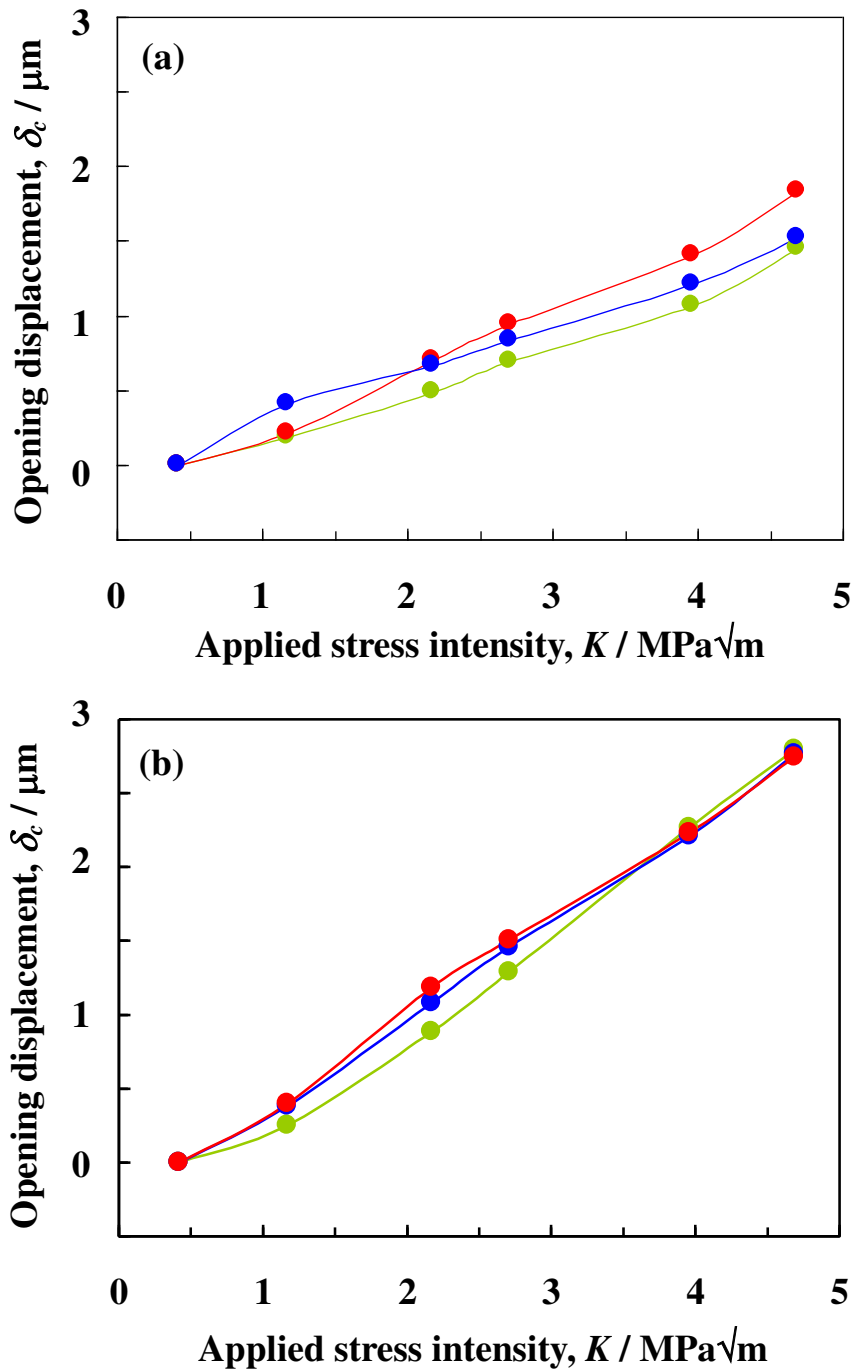


Fig.9 Variations of local opening displacement, δ_c , as a function of applied stress intensity measured utilizing centroid spacing of each pair of pores. (a) and (b) were measured about 170 ~ 250 μm and 350 ~ 460 μm from a crack-tip, respectively.

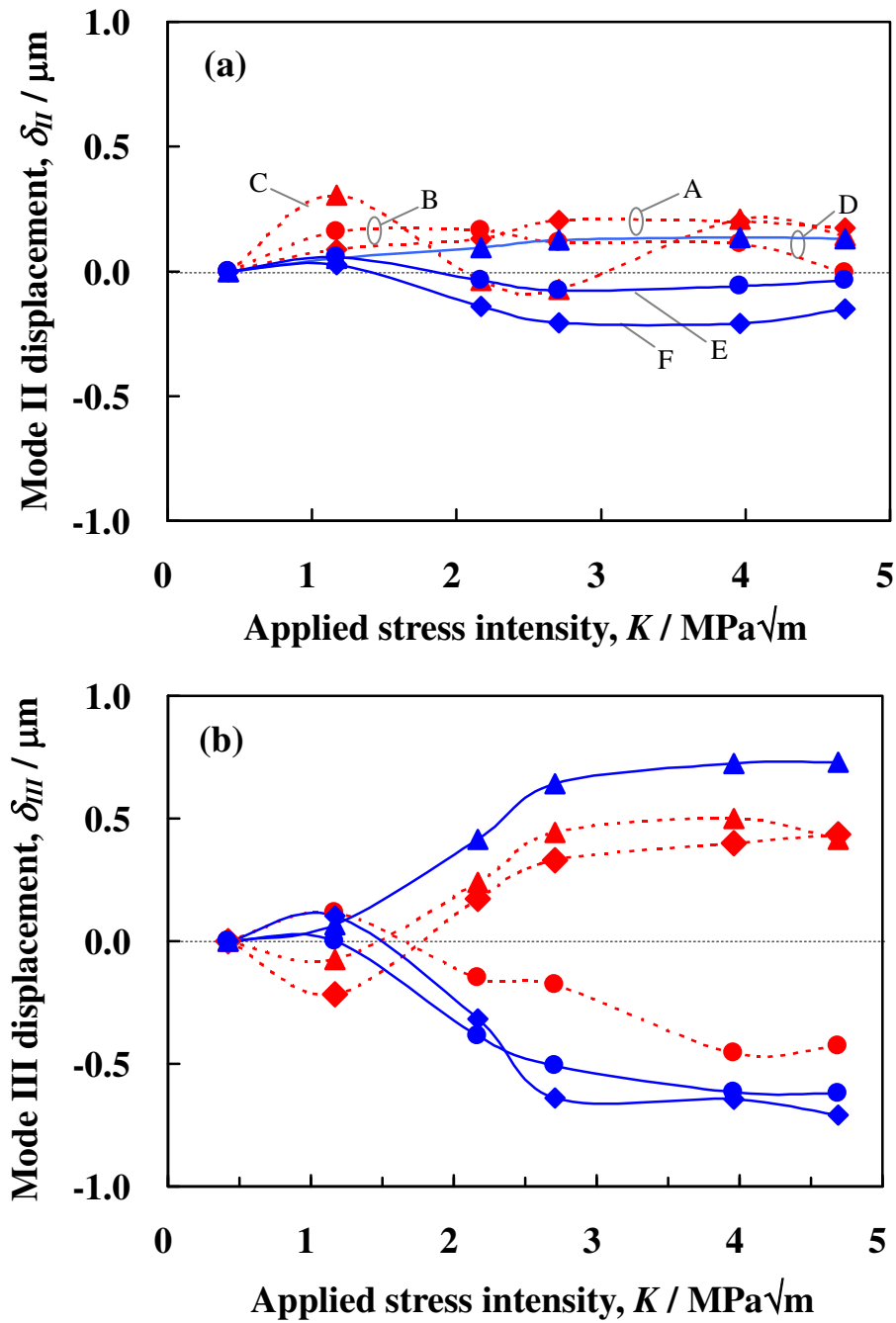


Fig.10 Variations of (a) mode II displacement, δ_{II} , and (b) mode III displacement, δ_{III} , as a function of applied stress intensity measured utilizing centroid spacing of each pair of pores. Points A ~ F correspond to those in Fig.9 respectively.

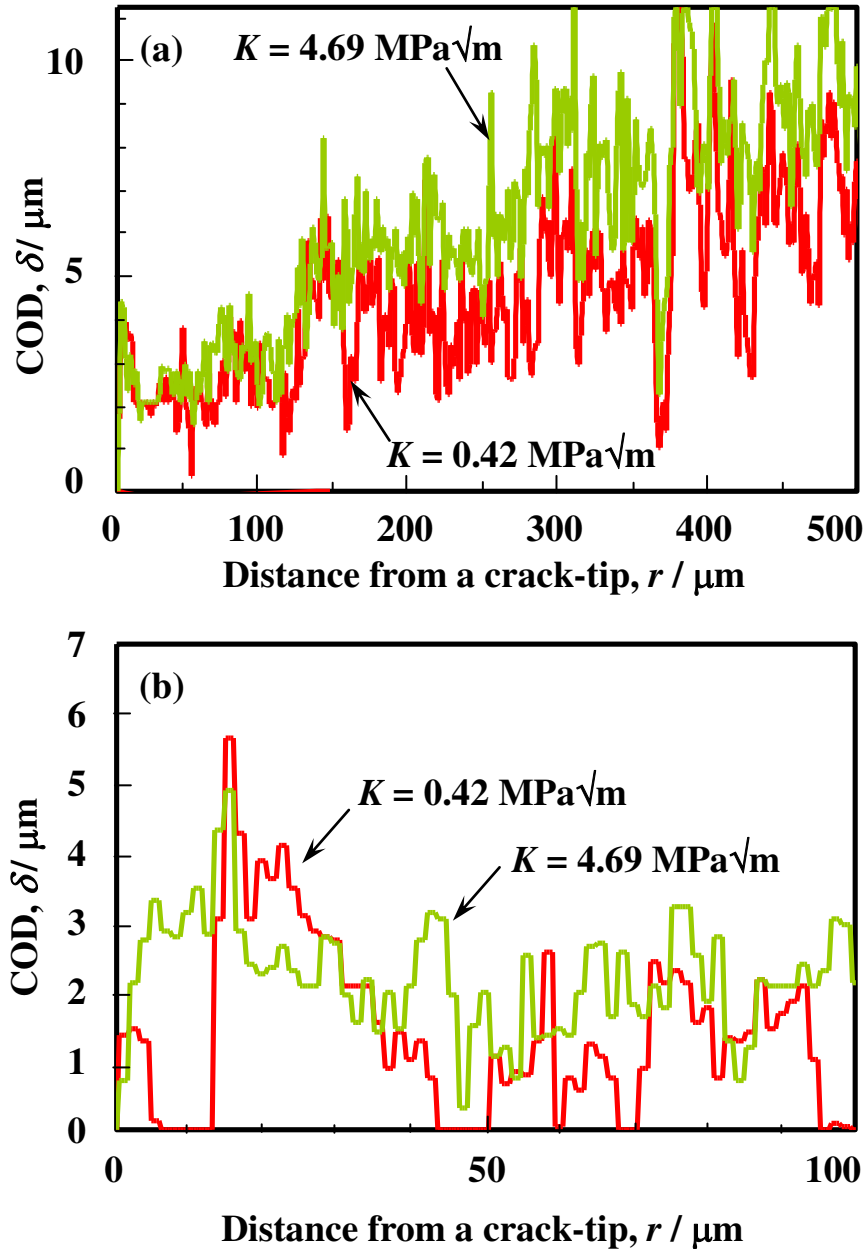


Fig. 11 COD profiles on two different cross-sections plotted from a crack-tip backwards. The ray casting algorithm was utilized for the measurements. (a) is a typical profile almost over the whole crack, while small points of fracture surface contact were observed in the vicinity of the crack-tip in (b).

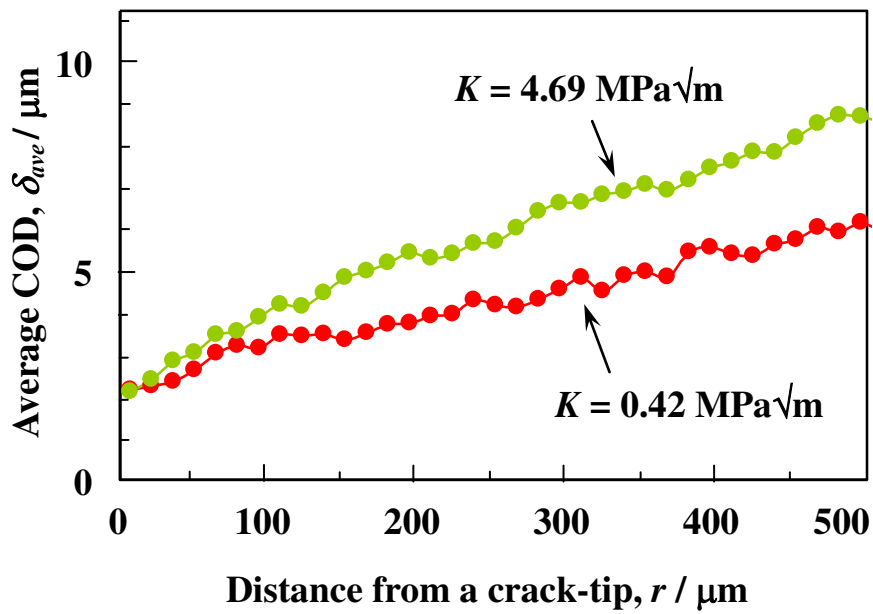


Fig. 12 COD profiles after averaging the COD data over the whole crack plotted as a function of distance from a crack-tip.